Sulfidation of Single Molecular Sheets of MoO_3 Pillared by Bipyridine in Nanohybrid MoO_3(4,4′-bipyridyl)$_{0.5}$

Xu Ming Wei and Hua Chun Zeng*

Department of Chemical and Environmental Engineering, Faculty of Engineering, National University of Singapore, 10 Kent Ridge Crescent, Singapore 119260

Received July 31, 2002. Revised Manuscript Received October 24, 2002

Individual sheets of MoO_3 in MoO_3(4,4′-bipyridyl)$_{0.5}$ (basal spacing $d_{002} = 1.12$ nm) can be considered as two-dimensional (2D) inorganic "macromolecules" while the interlayer organic ligands can be viewed as "pillars" to support or as "threads" to suspend these 2D host planes. This work concerns a sulfidation investigation of single molecular sheets of MoO_3 in the single crystals of the above compound under a H_2S/H_2 stream with various characterization methods. It is found that at a temperature as low as 100 °C, formation of surface H_xMoO_3-(4,4′-bipyridyl)$_{0.5}$ commences. A surface product of $MoO_{2-x}S_x$ is also observed throughout 100−200 °C. At 250 °C, all these intermediate phases are transformed completely to a final phase MoS_2(4,4′-bipyridyl)$_{0.2}$ (basal spacing $d_{001'} = 1.02$ nm) accompanying a partial deintercalation (from 0.5 down to 0.2) of 4,4′-bipyridine molecules from the interlayer space. In this connection, 4,4′-bipyridine molecules change from a standing configuration to a lying one after this sulfidation process. Although this new phase is thermally stable at its formation temperature (250 °C), inter-slab condensation of MoS_2 (basal spacing $d_{002} = 0.62$ nm) can also be observed in the topmost surface region. A mechanism based on these findings is also proposed. As demonstrated in this work, sulfurizing single molecular sheets of MoO_3 in existing MoO_3-containing layered compounds would also serve as a new means for synthesis of lamellar organic−inorganic nanohybrids comprising building units of transition metal dichalcogenides.

Introduction

Molybdenum has a wide variety of oxidation states and stereochemistries when combined with nonmetal elements or coordinated with inorganic or organic ligands.[1] Regarding its technological applications and fundamental interests, molybdenum trioxide MoO_3 and molybdenum disulfide MoS_2,[2−5] perhaps, are the two most important layered compounds when it is combined with group VI elements in the *p*-block of the periodic table, though both are the simplest compounds regarding their chemical composition.

Many polytypes of these two layered-compounds have been known. For example, orthorhombic MoO_3 (α-phase) is a thermodynamically stable phase, compared to other phases such as metastable monoclinic β-MoO_3 which has a ReO_3-type structure.[6−8] The α-MoO_3 has lamellar structure consisting of edge- and corner-linked distorted MoO_6 octahedra (two-dimensional "molecular sheet" of MoO_3).[6] There are two basic polytypes of MoS_2, hexagonal 2H−MoS_2 and rhombohedral 3R−MoS_2, owing to different stacking sequences.[9−13] In 2H−MoS_2, for example, the molybdenum atoms in the MoS_2 sheets are surrounded by six sulfur atoms, resulting in a trigonal prismatic coordination.[5,14,15]

Both MoO_3 and MoS_2 are widely used in industry as catalysts, display-devices, sensors, smart-windows, lubricants, battery-electrodes, and nanostructured materials in the latest context.[16−40] Concerning the formation

* To whom correspondence should be addressed. E-mail: chezhc@nus.edu.sg.

(1) Cotton, F. A.; Wilkinson, G. *Advanced Inorganic Chemistry*, 4th ed.; John Willey & Sons: New York, 1980; Ch. 22, p 844.
(2) Haber, J. In *Molybdenum: An Outline of Its Chemistry and Uses*; Braithwaite, E. R., Haber, J., Eds.; Elsevier Science: Amsterdam, The Netherlands, 1994; Ch. 10, p 479.
(3) Haber, J. In *Molybdenum: An Outline of Its Chemistry and Uses*; Braithwaite, E. R., Haber, J., Eds.; Elsevier Science: Amsterdam, The Netherlands, 1994; Ch. 10, p 494.
(4) Haber, J.; Lalik, E. *Catal. Today* **1997**, *33*, 119.
(5) Tenne, R.; Homyonfer, M.; Feldman, Y. *Chem. Mater.* **1998**, *10*, 3225 and references therein.
(6) Kihlborg, L. *Arkiv Kemi* **1963**, *21*, 357.
(7) Chen, M.; Waghmare, U. V.; Friend, C. M.; Kaxiras, E. *J. Chem. Phys.* **1998**, *109*, 6854.
(8) Queeney, K. T.; Friend, C. M. *J. Phys. Chem. B* **2000**, *104*, 409.
(9) Dickinson, R. G.; Pauling, L. *J. Am. Chem. Soc.* **1923**, *45*, 1466.
(10) Bell, R. E.; Herfert, R. E. *J. Am. Chem. Soc.* **1957**, *79*, 3351.
(11) Jellinek, R.; Bauerand, G.; Muller, H. *Nature* **1960**, *185*, 376.
(12) Wickman, F. E.; Smith, D. K. *Am. Mineral.* **1970**, *55*, 1843.
(13) Viswanath, R. N.; Ramasamy, S. *J. Mater. Sci.* **1990**, *25*, 5029.
(14) Cristol, S.; Paul, J. F.; Payen, E.; Bougeard, D.; Clemendot, S.; Hutschka, F. *J. Phys. Chem. B* **2000**, *104*, 11220.
(15) Park, K. T.; Kong, J.; Klier, K. *J. Phys. Chem. B* **2000**, *104*, 3145.
(16) Sabu, K. R.; Rao, K. V.; Nair, C. G. R. *Indian J. Chem.* **1994**, *33B*, 1053.
(17) Fournier, M.; Aouissi, A.; Rocchiccioli-Deltcheff, C. *J. Chem. Soc., Chem. Commun.* **1994**, *3*, 307.
(18) Hayashi, H.; Sugiyama, S.; Masaoka, N.; Shigemoto, N. *Ind. Eng. Chem. Res.* **1995**, *34*, 137.
(19) Günther, S.; Marsi, M.; Kolmakov, A.; Kiskinova, M.; Noeske, M.; Taglauer, E.; Mestl, G.; Schubert, U. A.; Knözinger, H. *J. Phys. Chem. B* **1997**, *101*, 10004.
(20) Takenaka, S.; Tanaka, T.; Funabiki, T.; Yoshida, S. *J. Phys. Chem. B* **1998**, *102*, 2960.
(21) Thorne, R. E. *Phys. Today* **1996**, *49*, 42.
(22) Tagaya, H.; Ara, K.; Kadokawa, J. I.; Karasu, M.; Chiba, K. *J. Mater. Chem.* **1994**, *4*, 551.

10.1021/cm020781y CCC: $25.00
Published on Web 12/31/2002

of MoS_2, sulfurizing conversion of MoO_3 to MoS_2 represents one of the most important chemical processes in their complex chemistries.[34−37] For example, sublimated MoO_3 nanoparticles in the size of <100 nm can be converted into nested inorganic fullerene-like 2H−MoS_2 in $H_2S/H_2/N_2$ gas.[38,39] This conversion takes place within seconds to tens of minutes depending on the number of MoS_2 slabs formed on the reduced oxide (e.g., MoO_{3-x} or MoO_2) substrates. The conversion commences as sulfur substitutes oxygen (Mo═O or Mo−O) at the outer oxide surface, and the internal bulk sulfidation is immediately followed when H_2S diffuses through the defects of outer layers of the resultant MoS_2 shells.[38,39]

Using a single molecular sheet for the in-depth investigation of $MoO_3 \rightarrow MoS_2$ is fundamentally desirable, because it offers us a unique opportunity to examine the ultimate "molecular" dimension of the layered solids in the above sulfidation processes. Ideally, a molecular sheet in this type of model investigation should have only minimum contact and interaction with its surroundings in order to be considered as a two-dimensional inorganic "macromolecule". With the recent developments in the field of nanohybrid materials,[40−49]

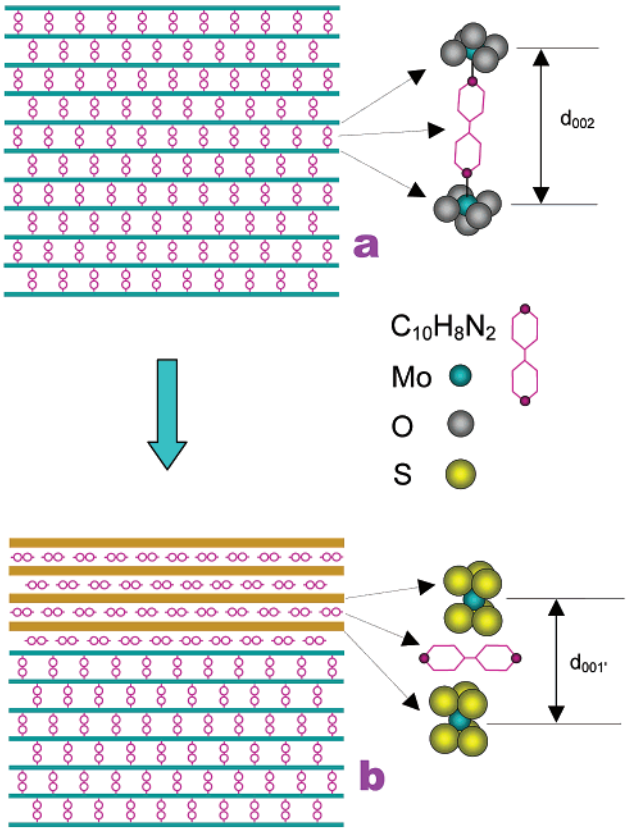

Figure 1. Schematic representation of sulfidation process of $MoO_3(4,4'\text{-bipyridyl})_{0.5}$ (a) to $MoS_2(4,4'\text{-bipyridyl})_{0.2}$ (b) under H_2S/H_2 stream. The intermediate compound $H_xMoO_3(4,4'\text{-bipyridyl})_{0.5}$ is not shown here because of its small quantity (see text).

it has been brought to our attention that the high-degree separation of individual molecular sheets of MoO_3 can be actually realized with a variety of organic−inorganic hybrid compounds, in which organic ligands or intercalants can be viewed as "pillars" to support or as "threads" to suspend the molecular sheets of MoO_3 in a three-dimensional space. In the present article, as a part of our recent effort in investigation of MoO_3 reduction and sulfidation,[50−52] we will report a mechanistic study on sulfidation process of MoO_3 molecular sheets supported by standing 4,4′-bipyridine molecules with a MoO_3-to-bipyridine molar ratio of 2:1, as illustrated in Figure 1. To the best of our knowledge, this is the first sulfidation investigation on an isolated molecular sheet of MoO_3. Because of a large interlayer space, hydrogen or sulfur species can access both sides of a single MoO_3 molecular sheet during the reactions, and apparently, the sulfidation processes in this model system seem to be different from those of bulk phase processes. Furthermore, we have also noticed that studies on inter-

(23) Wang, J.; Rose, K. C.; Lieber, C. M. *J. Phys. Chem. B* **1999**, *103*, 8405.
(24) Carcia, P. F.; McCarron, E. M., III. *Thin Solid Films* **1987**, *155*, 53.
(25) Yang, Y. A.; Cao, Y. W.; Loo, B. H.; Yao, J. N. *J. Phys. Chem. B* **1998**, *102*, 9392 and references therein.
(26) Kerr, T. A.; Leroux, F.; Nazar, L. F. *Chem. Mater.* **1998**, *10*, 2588.
(27) Tachibana, H.; Yamanaka, Y.; Sakai, H.; Abe, M.; Matsumoto, M. *Chem. Mater.* **2000**, *12*, 854.
(28) Brenner, J.; Marshall, C. L.; Ellis, L.; Tomczyk, N.; Heising, J.; Kanatzidis, M. *Chem. Mater.* **1998**, *10*, 1244.
(29) Ollivier, P. J.; Kovtyukhova, N. I.; Keller, S. W.; Mallouk, T. E. *Chem. Commun.* **1998**, 1563.
(30) Chhowalla, M.; Amaratunga, G. A. J. *Nature* **2000**, *407*, 164.
(31) Remskar, M.; Mrzel, A.; Skraba, Z.; Jesih, A.; Ceh, M.; Demsar, J.; Stadelmann, P.; Levy, F.; Mihailovic, D. *Science* **2001**, *292*, 479.
(32) Chen, J.; Kuriyama, N.; Yuan, H.; Takeshita, H. T.; Sakai, T. *J. Am. Chem. Soc.* **2001**, *123*, 11813.
(33) Zak, A.; Feldman, Y.; Lyakhovitskaya, V.; Leitus, G.; Popovitz-Biro, R.; Wachtel, E.; Cohen, H.; Reich, S.; Tenne, R. *J. Am. Chem. Soc.* **2002**, *124*, 4747 and references therein.
(34) Feldman, Y.; Wasserman, E.; Srolovitz, D. J.; Tenne, R. *Science* **1995**, *267*, 222.
(35) (a) Whitehurst, D. H.; Isoda, T.; Mochida, I. *Adv. Catal.* **1998**, *42*, 345. (b) Kushmerick, J. G.; Kandel, S. A.; Han, P.; Johnson, J. A.; Weiss, P. S. *J. Phys. Chem.* **2000**, *104*, 2980.
(36) (a) Gunther, S.; Gregoratti, L.; Kiskinova, M.; Taglauer, E.; Grotz, P.; Schubert, U. A.; Knözinger, H. *J. Chem. Phys.* **2000**, *112*, 5440. (b) Mestl, G.; Knözinger, H. *Langmuir* **1998**, *14*, 3964. (c) Muijsers, J. C.; Weber, Th.; van Hardeveld, R. M.; Zandbergen, H. W.; Niemantsverdriet, J. W. *J. Catal.* **1995**, *157*, 698.
(37) de Jong, A. M.; Borg, H. J.; van Ijzendoorn, L. J.; Soudant, V. G. F. M.; de Beer, V. H. J.; van Veen, J. A. R.; Niemantsverdriet, J. W. *J. Phys. Chem.* **1993**, *97*, 6477 and the references for XPS assignments therein.
(38) Feldman, Y.; Frey, G. L.; Homyonfer, M.; Lyakhovitskaya, V.; Margulis, L.; Cohen, H.; Hodes, G.; Hutchison, J. L.; Tenne, R. *J. Am. Chem. Soc.* **1996**, *118*, 5362.
(39) Zak, A.; Feldman, Y.; Alperovich, V.; Rosentsveig, R.; Tenne, R. *J. Am. Chem. Soc.* **2000**, *122*, 11108.
(40) Wang, Y.; Chen, J. S.; Xin, M. H.; Xu, R. R. *Inorg. Chem. Commun.* **1999**, *3*, 129.
(41) Gomez-Romero, P. *Adv. Mater.* **2001**, *13*, 163 and references therein.
(42) Roman, P.; Luque, A.; Gutierrez-Zorrilla, J. M. *Polyhedron* **1991**, *10*, 2057.
(43) Hagrman, D.; Zubieta, C.; Rose, D. J.; Zubieta, J.; Haushalter, R. C. *Angew. Chem., Int. Ed. Engl.* **1997**, *36*, 873.
(44) Guillou, N.; Ferey, G. *J. Solid State Chem.* **1999**, *147*, 240.
(45) Shao, K.; Ma, Y.; Cao, Y. A.; Chen, Z. H.; Ji, X. H.; Yao, J. N. *Chem. Mater.* **2001**, *13*, 250.
(46) Xu, Z. P.; Zeng, H. C. *J. Phys. Chem. B* **2000**, *104*, 10206.
(47) Xu, Z. P.; Xu, R.; Zeng, H. C. *Nano Lett.* **2001**, *1*, 703.
(48) Ozin, G. A. *Adv. Mater.* **1992**, *4*, 612.
(49) Hagrman, P. J.; LaDuca, R. L., Jr.; Koo, H. J.; Rarig, R., Jr.; Haushalter, R. C.; Whangbo, M. H.; Zubieta, J. *Inorg. Chem.* **2000**, *39*, 4311.
(50) Hsu, Z. Y.; Zeng, H. C. *J. Phys. Chem. B* **2000**, *104*, 11891.
(51) (a) Zeng, H. C.; Ng, W. K.; Cheong, L. H.; Xie, F.; Xu, R. *J. Phys. Chem. B* **2001**, *105*, 7178. (b) Zeng, H. C.; Xie, F.; Wong, K. C.; Mitchell, K. A. R. *Chem. Mater.* **2002**, *14*, 1788.
(52) (a) Lauhon, L. J.; Ho, W. *J. Phys. Chem. B* **2001**, *105*, 3987. (b) Travert, A.; Manoilova, O. V.; Tsyganenko, A. A.; Maugé, F.; Lavalley, J. C. *J. Phys. Chem. B* **2002**, *106*, 1350. (c) Michalides, A.; Hu, P. *J. Chem. Phys.* **2001**, *115*, 8570. (d) Sierraalta, A.; Herize, A.; Añez, R. *J. Phys. Chem. A* **2001**, *105*, 6519.

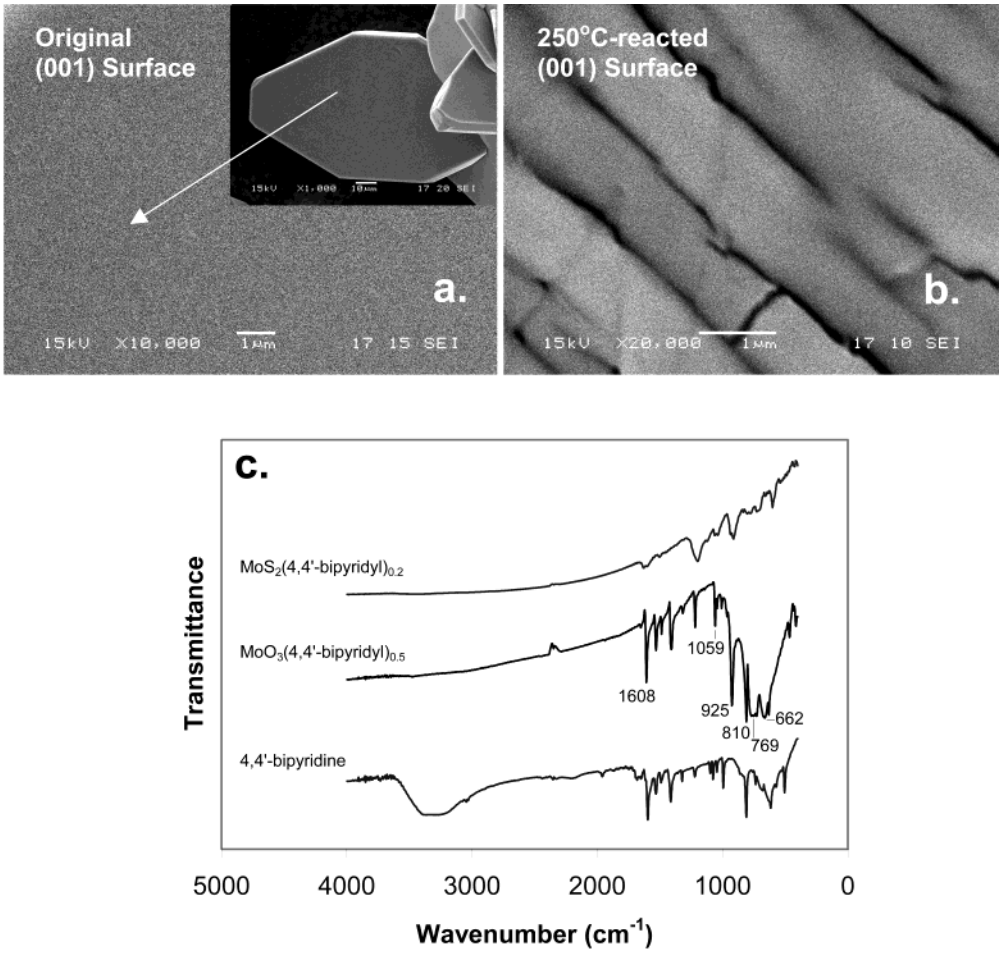

Figure 2. Representative SEM images and FTIR spectra: (a) as-prepared MoO_3(4,4′-bipyridyl)$_{0.5}$ crystals (original); (b) MoO_3-(4,4′-bipyridyl)$_{0.5}$ crystals reacted in the H_2S/H_2 stream at 250 °C for 1 h; and (c) FTIR spectra of 4,4′-bipyridine, MoO_3(4,4′-bipyridyl)$_{0.5}$, and MoS_2(4,4′-bipyridyl)$_{0.2}$ (produced from sulfidation of MoO_3(4,4′-bipyridyl)$_{0.5}$ in the H_2S/H_2 stream at 250 °C for 6 h).

calation of large organic compounds/polymers into the MoS_2 host structure have been very limited so far,[27−29] compared to those for existing metal/inorganic−MoS_2 intercalated compounds.[33,53−57] In addition to the prevailing exfoliation-then-restacking methods,[27−29,40] therefore, our method by sulfurizing single molecular sheets of MoO_3 would also serve as a new means for synthesis of lamellar organic−inorganic nanohybrids comprising building units of transition metal dichalcogenides.

Experimental Section

The preparation method for MoO_3(4,4′-bipyridyl)$_{0.5}$ adopted in this work is similar to a previously reported procedure.[49] Briefly, a solid−liquid mixture of α-MoO_3 (0.12 g, Aldrich, >99.5%), 4,4′-bipyridine (0.13 g, $C_{10}H_8N_2$, Fluka, >99%), and deionized water (15 g) was transferred to a Teflon-lined stainless steel autoclave. The hydrothermal reactions were conducted at 150 °C for 72 h, which was then followed by a thorough washing with deionized wate and drying at room temperature for the reaction products. The yellowish single crystals of MoO_3(4,4′-bipyridyl)$_{0.5}$ are well faceted with low Miller index crystal planes ({001} planes are the largest among all, Figure 2); the size of crystallites is in the range of 50−250 μm.

The as-grown MoO_3(4,4′-bipyridyl)$_{0.5}$ crystals were then used as single molecular sheets for sulfidation investigation. The reactions were carried out in a tubular quartz reactor (4 mm i.d.) at 100−250 °C (with a 50-°C interval) using a H_2S/H_2 stream (H_2S 15 mol % + H_2 85 mol %) under normal atmospheric pressure. The temperature of the reactor was monitored with a K-type thermocouple. The heating and cooling rates were kept the same at 10 °C/min, and a small gas flowrate of 15 mL min^{-1} (controlled by a mass-flow control system, Brooks 5950) was used to reduce concentration gradient of the input H_2S/H_2 stream across the sample zone (16−19 mg of the as-prepared crystals; placed in the central part of the reactor). The off-gas was introduced to a $ZnSO_4$ solution to remove unreacted H_2S before it was vented into the atmosphere. The sulfidation reaction time was set at 1 h for most experiments, although a longer reaction time of up to 6 h had also been adopted.

Elemental analysis for carbon, hydrogen, and nitrogen contents in the prepared crystal sample MoO_3(4,4′-bipyridyl)$_{0.5}$ was carried out with a Perkin-Elmer 2400 CHN-analyzer. The atomic ratio of Mo to S in the sulfurized product MoS_2(4,4′-bipyridyl)$_{0.2}$ was determined with energy dispersive spectroscopy (EDX, JSM-5600LV) after partial removal of the bipyridine intercalants. Crystallographic information of samples was investigated with powder X-ray diffraction (XRD; Shimadzu XRD-6000, Cu Kα radiation, $\lambda = 1.5406$ Å). Crystal powders of the samples were estimated from full-width-at-half-maxi-

(53) Rudorff, W. *Chimia* **1965**, *19*, 489.
(54) Somoano, R. B.; Hadek, V.; Rembaum, A. *J. Chem. Phys.* **1973**, *58*, 697.
(55) Heising, J.; Kanatzidis, M. G. *J. Am. Chem. Soc.* **1999**, *121*, 11720.
(56) Dungey, K. E.; Curtis, M. D.; Penner-Hahn, J. E. *Chem. Mater.* **1998**, *10*, 2152.
(57) Alexiev, V.; Meyer zu Altenschildesche, H.; Prins, R.; Weber, Th. *Chem. Mater.* **1999**, *11*, 1742.

mums (fwhms) of some intense XRD diffraction peaks using Scherrer's method.[58] Surface topography of the crystal samples was examined before and after the sulfidation reactions with scanning electron microscopy (SEM, JEOL, JSM-5600LV, 15 kV). Thermal stability of the as-prepared MoO_3(4,4′-bipyridyl)$_{0.5}$ and the sulfurized product MoS_2(4,4′-bipyridyl)$_{0.2}$ was investigated with thermogravimetric and differential-thermogravimetric analysis (TGA/DTG, Shimadzu TGA-50) at a heating rate of 10 °C min^{-1} respectively in oxidative and inert atmospheres (air and nitrogen respectively; 50 mL min^{-1}).[59,60] MoO_3(4,4′-bipyridyl)$_{0.5}$ and MoS_2(4,4′-bipyridyl)$_{0.2}$ powders, together with 4,4′-bipyridine for reference, were investigated with Fourier transform infrared spectroscopy (FTIR; FTS135, Bio-Rad). The potassium bromide (KBr) pellet technique was employed to hold the samples (1 wt %).[49] Each FTIR spectrum was collected after 100 scans with a resolution of 2 cm^{-1}.

Surface compositional evolutions of the reacted MoO_3(4,4′-bipyridyl)$_{0.5}$ crystals were investigated with X-ray photoelectron spectroscopy (XPS; AXIS-Hsi, Kratos Analytical) using a monochromatized Al Kα exciting radiation ($h\nu = 1486.71$ eV). Transfer of the reacted crystals from the quartz reactor into the XPS sample chamber was handled under air atmosphere at room temperature. The XPS spectra of all studied elements were measured with a constant analyzer-pass-energy of 40.0 eV. All binding energies (BE) were referenced to the C 1s peak (BE = 284.7 eV) arising from adventitious carbon.[61−65] Prior to the peak deconvolution, X-ray satellites and inelastic background (Shirley-type) were subtracted for all spectra, as done in our previous XPS investigations.[51] High-resolution analytical transmission electron microscopy (TEM, JEM-2010, 200 kV) was used to examine the layered structure of the final sulfurized products. The specimens for TEM imaging and selected area electron diffraction (SAED) studies were prepared by suspending solid samples in acetone, and related technical details can be found in our previous publications.[66]

Results and Discussion

Powder XRD structural analysis and CHN measurement confirm that the as-prepared single crystals are in crystallographic structure of monoclinic symmetry (space group $P2_1/c$) with a weight (wt) ratio of C/H/N = 26.80 wt %/1.85 wt %/6.22 wt % identical to the expected values for the stoichiometric compound.[49] Thermal stability of this compound has been further tested with the TGA method. It is found that MoO_3(4,4′-bipyridyl)$_{0.5}$ does not show any weight loss until 330−380 °C in either air or nitrogen atmosphere. On the basis of the TGA data for the intercalant 4,4′-bipyridine (massive weight losses of 34.656 wt % at 421 °C in air and of 34.594 wt % at 435 °C in nitrogen), the chemical stoichiometry and high thermal stability of this organic−inorganic hybrid precursor are once again verified. Figure 2a shows the crystal morphology of MoO_3(4,4′-bipyridyl)$_{0.5}$ prepared in our work. The IR absorptions of this compound (Figure 2c) at 1608, 1059, 925, 810, 769, and 662 cm^{-1} are identical to the reported data.[49] The layered structure of this compound is clearly evidenced with the (00*l*) reflections in the XRD pattern

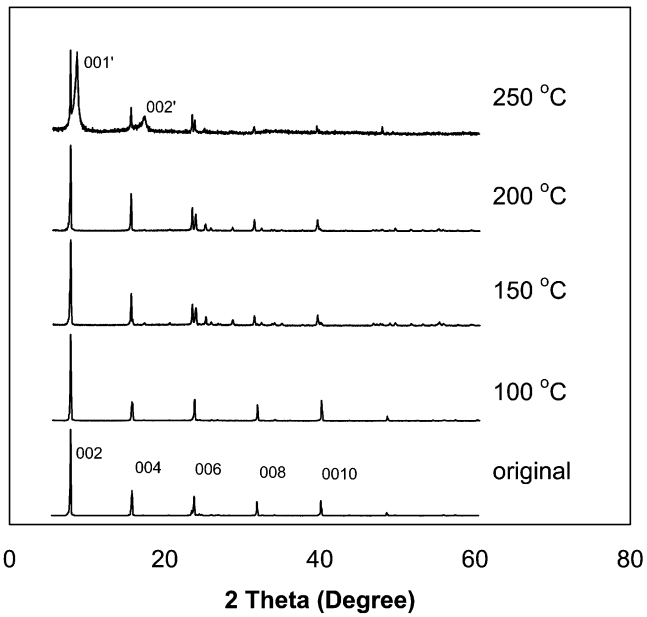

Figure 3. Powder XRD patterns of as-prepared MoO_3(4,4′-bipyridyl)$_{0.5}$ crystals and their reacted samples in the H_2S/H_2 stream at 100−250 °C for 1 h. Prime sign denotes the new reflections from MoS_2(4,4′-bipyridyl)$_{0.2}$ phase, and the peaks are indexed following those used for organic−inorganic layered hybrids.[27,41]

of Figure 3. The hydrothermal synthesis involves an insertion of 4,4′-bipyridine into basal-sheets of orthorhombic α-MoO_3. With the pillaring of this bidentate ligand (Figure 1a), the interlayer space between two basal-sheets expands from the original 0.693 nm ($d_{010}/2 = b/2$; α-MoO_3) to 1.12 nm ($d_{002} = c/2$; MoO_3(4,4′-bipyridyl)$_{0.5}$). The direct coordination of nitrogen to the metal cations, in replacing one of the oxygen atoms, converts partially corner-sharing MoO_6 octahedra into entirely corner-sharing MoO_5N octahedra in MoO_3(4,4′-bipyridyl)$_{0.5}$ (Figure 1a), noting that the octahedra of α-MoO_3 are both edge- and corner-sharing in their double-layered sheets.

In view of the disappearance of the double-layered structure, MoO_3 molecular sheets pillared in MoO_3(4,4′-bipyridyl)$_{0.5}$ seem to be more prone to the sulfidation reactions, as the molybdenum atom is now sitting on the base of a distorted pyramid formed by five oxygen atoms if one ignores the coordinated bonding between Mo and bipyridine (Mo−N = 0.241 nm, the longest bond among the six bonds in a MoO_5N octahedron).[49] Possible reactions between MoO_3 molecular sheets in MoO_3(4,4′-bipyridyl)$_{0.5}$ hybrid and H_2S/H_2 at the studied temperatures can be listed below in analogy to the bulk reactions:[34,37,39,51,52,67−75]

(58) Cheetham, A. K.; Day, P. *Solid-State Chemistry: Techniques*; Clarendon Press: Oxford, 1987; p 79.
(59) Ji, L.; Lin, J.; Zeng, H. C. *J. Phys. Chem. B* **2000**, *104*, 1783.
(60) Xu, Z. P.; Zeng, H. C. *Chem. Mater.* **2001**, *13*, 4564.
(61) Wager, C. D. *J. Electron Spectrosc. Relat. Phenom.* **1980**, *18*, 345.
(62) Bird, R. J.; Swift, P. *J. Electron. Spectrosc.* **1980**, *21*, 227.
(63) Swift, P. *Surf. Interface Anal.* **1982**, *4*, 47.
(64) Kohiki, S. *Appl. Surf. Sci.* **1984**, *17*, 297.
(65) Barr, T. L.; Seal, S. *J. Vac. Sci. Technol. A* **1995**, *13*, 1239.
(66) Sampanthar, J. T.; Zeng, H. C. *J. Am. Chem. Soc.* **2002**, *124*, 6668.
(67) Birtill, J. J.; Dickens, P. G. *Mater. Res. Bull.* **1978**, *13*, 311.
(68) Dickens, P. G.; Birtill, J. J.; Wright, C. J. *J. Solid State Chem.* **1979**, *28*, 185.
(69) Slade, R. C. T.; Halstead, T. K.; Dickens, P. G. *J. Solid State Chem.* **1980**, *34*, 183.
(70) Ritter, C.; Müller-Warmuth, W.; Schöllhorn, R. *J. Chem. Phys.* **1985**, *83*, 6130.
(71) Dickens, P. G.; Crouch-Baker, S.; Weller, M. T. *Solid State Ionics* **1986**, *18 & 19*, 89.
(72) Sotani, N.; Eda, K.; Kunitomo, M. *J. Chem. Soc., Faraday Trans.* **1990**, *86*, 1583.
(73) Eda, K. *J. Mater. Chem.* **1992**, *2*, 533.
(74) Weber, Th.; Muijsers, J. C.; Niemantsverdriet, J. W. *J. Phys. Chem.* **1995**, *99*, 9194.

$$MoO_3 + x/2\ H_2S = H_xMoO_3 + x/2\ S \quad (1)$$

$$MoO_3 + xH_2S = MoO_{3-x}S_x + xH_2O \quad (2)$$

$$MoO_3 + 3H_2S = MoS_3 + 3H_2O \quad (3)$$

$$MoS_3 = MoS_2 + S \quad (4)$$

$$MoO_3 + H_2S = MoO_2 + H_2O + S \quad (5)$$

$$MoO_2 + xH_2S = MoO_{2-x}S_x + xH_2O \quad (6)$$

$$MoO_2 + 2H_2S = MoS_2 + 2H_2O \quad (7)$$

As our reactions were conducted at ≤250 °C, using H_2 as a reducing agent for the above reactions is not plausible because reduction of MoO_3 with H_2 is observed only at temperatures greater than 350 °C.[76] On the other hand, we had recently observed that reaction 1 can take place on the (010) surface of single crystal α-MoO_3 in a H_2S (balanced with H_2) stream at only ∼150 °C.[51]

The sulfidation process has been investigated as a function of temperature. Figure 2 reports a surface morphology change upon the sulfidation reactions, viewed along the *c*-axis of the crystals. Although no peeling is observed, lateral shrinkage of the (00*l*) planes is seen (starting at 150 °C), which indicates the possible solid−gas reactions (e.g., eqs 1 to 7) had taken place. The crystal surface becomes more divisive with increase of reaction temperature. Thermally induced stress, together with possible phase changes in the reactions, makes the as-prepared crystals more easily cleaved along other crystallographic directions. This is evidenced in our preparation of powders (from the reacted MoO_3(4,4′-bipyridyl)$_{0.5}$ crystals) for the XRD measurement. As can be seen, non-(00*l*) reflections are emerging in powder XRD patterns with increasing reaction temperature (≥150 °C). More surprisingly, a new set of (00*l*)′ reflections appears at 250 °C, which indicates a new layered-structure is formed at this temperature. Our XRD pattern analysis indicates that the original basal spacing of MoO_3(4,4′-bipyridyl)$_{0.5}$ is reduced from 1.12 to 1.02 nm in this newly derived structure (or 8.9% reduction). Although $d_{001'}$ is strictly equal to $2d_{002'}$, the reflection intensity of (00*l*)′ is attenuated significantly, especially for higher-order beams. Compared to the XRD pattern of MoO_3(4,4′-bipyridyl)$_{0.5}$, the lack of higher order peaks indicates that there is a configuration transformation of the intercalated 4,4′-bipyridine in the interlayer space at this reaction temperature (addressed further in later XRD/FTIR/XPS/TEM analyses). In particular, 4,4′-bipyridine might reorient itself from a standing configuration to a lying arrangement in the new layered structure (Figure 1b). The lying 4,4′-bipyridine molecules, though they could be arranged in either an ordered or a less-ordered manner, will still give (002)′ reflection, noting that the observed (002)′ reflection must include the contribution from the planes formed by interlayer species, as will be further discussed later.

In view of the above morphological and structural evolutions, it will be interesting to address the fundamental issues related to the reactions between the pillared molecular sheets and gaseous reductants. Regarding the actual sulfidation process, it must be noted that XRD is only a bulk technique, and surface reactions may occur at a temperature much lower than the XRD-detected 250 °C. Therefore, surface compositional analysis of reacted samples should allow us to acquire more detailed information. To this end, XPS is an excellent surface-sensitive tool for the current reaction system,[77] noting that its sampling depth of just a few nanometers will reveal the chemical changes of the topmost crystal slabs (the observed crystal basal spacing $d_{002} = 1.12$ nm and $d_{001'} = 1.02$ nm) in the present low-temperature sulfidation. It must be mentioned that sulfidation of MoO_3 has been investigated extensively with this surface technique over the past 30 years and a large volume of data, especially for the final product MoS_2, has been accumulated in the literature for reference.[15,27,37,38,78−88]

Figure 4 and Table 1 report our XPS analysis results for the MoO_3(4,4′-bipyridyl)$_{0.5}$ crystals after reactions in H_2S/H_2 at various temperatures. For each C 1s spectrum (Figure 4), the first peak at 284.7 eV is assigned to adventitious carbon,[61−65] and the second peak at 285.5−286.0 eV is assigned to the −C═C− in the conjugate ring structure of 4,4′-bipyridine.[89,90] It is interesting to note that the Mo 3d spectra measured from the pillared molecular MoO_3 sheets are similar to that measured from α-MoO_3, as expected for molybdenum in its highest oxidation state VI; the two peaks at 232.7 and 235.8 eV can be assigned to Mo $3d_{5/2}$ and Mo $3d_{3/2}$ branches of MoO_3 respectively.[37,51,76,78−80] At a temperature as low as 100 °C, formation of H_xMoO_3 (eq 1)[67−73] commences, as shown in the two smaller twin peaks at 231.0 and 234.1 eV.[51] This chemical phase has been recently confirmed at ∼150 °C with a combined approach of AFM/XRD/XPS for sulfidation on the (010) surface of single-crystal MoO_3, and the hydrogen source for such a proton attachment has been known from H_2S molecules at these low temperatures.[51] Because the present

(75) Homyonfer, M.; Mastai, Y.; Hershfinkel, M.; Volterra, V.; Hutchison, J. L.; Tenne, R. *J. Am. Chem. Soc.* **1996**, *118*, 7804.
(76) Spevack, P. A.; McIntyre, N. S. *J. Phys. Chem.* **1992**, *96*, 9029.
(77) Doron-Mor, I.; Hatzor, A.; Vaskevich, A.; van der Boom-Moav, T.; Shanzer, A.; Rubinstein, I.; Cohen, H. *Nature* **2000**, *406*, 382.
(78) Moulder, J. F.; Stickle, W. F.; Sobol, P. E.; Bomben, K. D. *Handbook of X-ray Photoelectron Spectroscopy: A Reference Book of Standard Spectra for Identification and Interpretation of XPS Data*; Chastain, J., Ed.; Perkin-Elmer Corporation, Physical Electronics Division; Imprint: Eden Prairie, MN, 1992.
(79) Protela, L.; Grange, P.; Delmon, B. *J. Catal.* **1995**, *156*, 243.
(80) Nagano, M.; Greenblatt, M. *J. Non-Cryst. Solids* **1988**, *101*, 255.
(81) Anwar, M.; Hogarth, C. A.; Bulpett, R. *J. Mater. Sci.* **1989**, *24*, 3087 and the references therein.
(82) Delporte, P.; Meunier, F.; Pham-Huu, C.; Vennegues, P.; Ledoux, M. J.; Guille, J. *Catal. Today* **1995**, *23*, 251.
(83) Braun, S.; Appel, L. G.; Camorim, V. L.; Schmal, M. *J. Phys. Chem. B* **2000**, *104*, 6584.
(84) Thurston, T. R.; Wilcoxon, J. P. *J. Phys. Chem. B* **1999**, *103*, 11.
(85) Liao, H.; Wang, Y.; Zhang, S.; Qian, Y. *Chem. Mater.* **2001**, *13*, 6.
(86) Hada, K.; Nagai, M.; Omi, S. *J. Phys. Chem. B* **2001**, *105*, 4084.
(87) (a) Rodriguez, J. A.; Dvorak, J.; Jirsak, T. *J. Phys. Chem. B* **2000**, *104*, 11515. (b) Rodriguez, J. A.; Liu, G.; Jirsak, T.; Hrbek, J.; Chang, Z.; Dvorak, J.; Maiti, A. *J. Am. Chem. Soc.* **2002**, *124*, 5242.
(88) Maugé, F.; Lamotte, J.; Nesterenko, N. S.; Manoilova, O.; Tsyganenko, A. A. *Catal. Today* **2001**, *70*, 271.
(89) Mitton, D. B.; Walton, J.; Thompson, G. E. *Surf. Interface Anal.* **1993**, *20*, 36.
(90) Sarno, D. M.; Jiang, B.; Grosfeld, D.; Afriyie, J. O.; Matienzo, L. J.; Jones, W. E., Jr. *Langmuir* **2000**, *16*, 6191.

Table 1. Binding Energies (in eV) of Elements for the Studied Samples Before and After Sulfidation Reactions[a]

element	25 °C[b]	100 °C[c]	150 °C[c]	200 °C[c]	250 °C[c]
C 1s (reference)	284.7	284.7	284.7	284.7	284.7
C 1s (−C═C−)	285.6	285.5	285.7	285.9	286.0
Mo $3d_{5/2}$ (MoO_3)	232.7	232.3	232.6	232.5	232.5
Mo $3d_{3/2}$ (MoO_3)	235.8	235.4	235.7	235.6	235.6
Mo $3d_{5/2}$ (H_xMoO_3)		231.0	231.1		
Mo $3d_{3/2}$ (H_xMoO_3)		234.1	234.2		
Mo $3d_{5/2}$ ($MoO_{2-x}S_x$)		229.4	229.4	229.3	
Mo $3d_{3/2}$ ($MoO_{2-x}S_x$)		232.5	232.5	232.4	
Mo $3d_{5/2}$ (MoS_2)					229.0
Mo $3d_{3/2}$ (MoS_2)					232.1
S 2s		226.6	227.2	226.9	226.1
S $2p_{3/2}$ (S)		163.4	163.3	163.3	163.3
S $2p_{1/2}$ (S)		164.5	164.5	164.5	164.4
S $2p_{3/2}$ (S^{2-} in $MoO_{2-x}S_x$ or MoS_2)		162.0	162.0	161.9	161.8
S $2p_{1/2}$ (S^{2-} in $MoO_{2-x}S_x$ or MoS_2)		163.1	163.1	163.1	163.0
S $2p_{3/2}$ (S^{6+} in SO_4^{2-})					168.1
S $2p_{1/2}$ (S^{6+} in SO_4^{2-})					169.2
N 1s (−N = to Mo)	399.4				
N 1s (−N = normal)		399.0	399.1	399.0	
N 1s (−N = with δ+)			400.8	401.4	401.2
Mo $3p_{3/2}$ (MoO_3)	398.2	398.4	398.2	398.2	398.5
Mo $3p_{3/2}$ (H_xMoO_3)		397.3	397.3		
Mo $3p_{3/2}$ ($MoO_{2-x}S_x$)		395.7	395.5	395.2	
Mo $3p_{3/2}$ (MoS_2)					394.9
O 1s (O^{2-})	530.3	529.8	530.0	530.7	530.7
O 1s (others)	531.2	530.8	531.2	531.8	531.7

[a] Single-crystal samples were used in XPS measurement (without powdering). [b] As-grown MoO_3(4,4′-bipyridyl)$_{0.5}$ single crystals before sulfidation. [c] Reacted MoO_3(4,4′-bipyridyl)$_{0.5}$ single crystals after sulfidation reactions at the respective temperatures for 1 h.

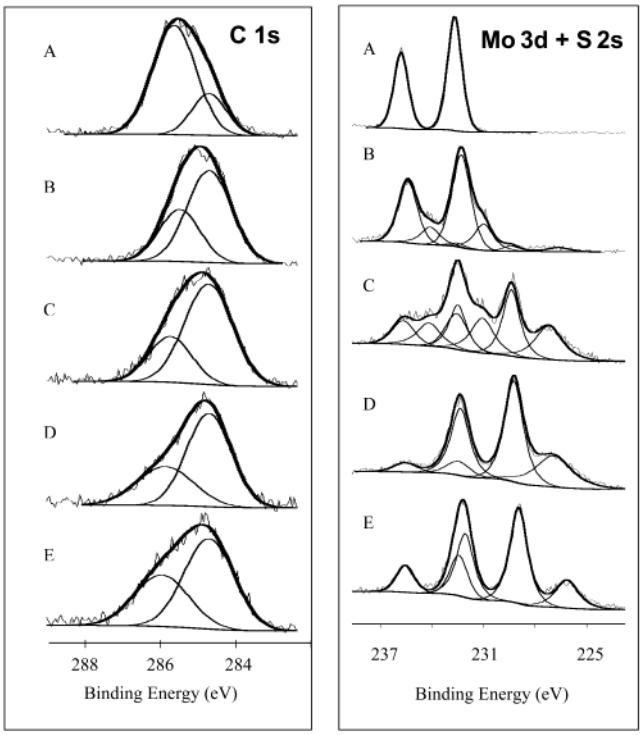

Figure 4. Representative XPS spectra of as-prepared MoO_3-(4,4′-bipyridyl)$_{0.5}$ crystals (A) and their reacted samples in the H_2S/H_2 stream at 100−250 °C (B, 100 °C; C, 150 °C; D, 200 °C; and E, 250 °C) for 1 h.

H_xMoO_3 is modified from the MoO_3 of MoO_3(4,4′-bipyridyl)$_{0.5}$, its sheets are still pillared by the 4,4′-bipyridine ligands. Strictly speaking, this surface phase is analogous to H_xMoO_3(4,4′-bipyridyl)$_{0.5}$ (where $x \approx 0.5$),[49] although its bulk phase is not formed. With introduction of protons into the MoO_3 sheets, the central atom molybdenum has been partially reduced (e.g., from Mo^{6+} to $Mo^{5.5+}$, when $x = 0.5$). The resulting compound H_xMoO_3(4,4′-bipyridyl)$_{0.5}$ essentially maintains the same network characteristic of the parent MoO_3(4,4′-bipyridyl)$_{0.5}$. For example, the angle between N···N′ axis of the bipyridine ligands and the molybdenum oxide planes is modified from the previous 85° in MoO_3(4,4′-bipyridyl)$_{0.5}$ to 90° in H_xMoO_3(4,4′-bipyridyl)$_{0.5}$.[49] Space group of the latter compound has been determined to be monoclinic $I2/m$ ($c/2 = 1.14$ nm), in which the proton is disordered over the bridging oxo groups.[49] In addition to this reduced state, formation of $MoO_{2-x}S_x$ is also observed. Though its relative intensity is very low, the shoulder at the low BE part of the spectrum can be deconvoluted into two even smaller peaks at 229.4 and 232.5 eV. These assignments are further elucidated in the spectra of Mo 3p and S 2p (Table 1). As can be seen, three subpeaks at the low Mo $3p_{3/2}$ BE range of 398.4 to 395.7 eV can be assigned respectively to the above three surface phases MoO_3, H_xMoO_3, and $MoO_{2-x}S_x$.[15,37,78−88] In good agreement with the latter two reduced phases, elemental sulfur S and lattice S^{2-} of $MoO_{2-x}S_x$ have also been detected for the 100-°C-reacted crystals. In particular, the elemental sulfur can be viewed as a reaction indicator, as it is a redox product when molybdenum is reduced from higher oxidation states (eqs 1−7). On the basis of these results, it is clear that all or some of eqs 1−7 on the crystal surfaces have been operative at 100 °C, although the bulk phase still remains intact, as shown in the XRD data (Figure 3). In particular, N 1s has shown a transition from a nitrogen−molybdenum type (i.e., coordination bonding between pyridyl ═N− and metal, BE = 399.4 eV,[90] Table 1) to a terminal type (i.e., normal unattended = N− end, BE = 399.0 eV,[90] Table 1), suggesting that a detachment of 4,4′-bipyridine "pillars" from the original MoO_3 sheets starts at this temperature. With heating at 150 °C, the $MoO_{2-x}S_x$ species in the surface region is further developed, which can be seen in the significant peak-area rises of Mo 3d and Mo 3p photoelectrons from

this phase (Table 1). In addition to the normal ═N− (399.1 eV), a more positive N 1s peak at 400.8 eV (═$N^{\delta+}$−) is detected, which indicates increasing interaction of the nitrogen of bipyridyl molecules with the MoS_2 slabs, as a result of this type of intercalation (effect of partial charge-transfer).[33,90] When the temperature is increased to 200 °C, the intermediate product H_xMoO_3 is no longer observed and the $MoO_{2-x}S_x$ is seen as a predominant surface phase. This observation can be attributed to a thicker $MoO_{2-x}S_x$ phase that covers H_xMoO_3 underneath formed at this reaction condition; the observed Mo^{VI} state will be addressed later. A greater degree of sulfidation is also evidenced with a substantial increase in S 2p peaks of the lattice sulfur S^{2-} at this temperature (Table 1). At 250 °C, the highest temperature employed in this study, the sulfidation reactions proceed to their maximum extent. There are at least three observations related to this reaction temperature. First, the normal ═N− is no longer observed, leaving only a ═$N^{\delta+}$− subpeak at 401.2 eV (Table 1). This indicates a complete disappearance of the unattended 4,4′-bipyridine. Second, the SO_4^{2-} species (Table 1) was likely formed from elemental sulfur via air oxidation during the XPS sample transfer, noting the high sulfur content in this sample.[87,88] Third, the $MoO_{2-x}S_x$ has been converted totally to MoS_2 (Table 1) at this temperature. Compared to the reaction product elemental sulfur S, the content of divalent S^{2-} anions is drastically increased. The O 1s data of O^{2-} species (Table 1) also support the above assignments for various surface phases.[15,37,78−88]

In excellent agreement with the above XPS findings, the new layered structure is also detected by XRD for the sample reacted at 250 °C. By comparing the relative intensities of basal plane reflections (d_{002} and $d_{001'}$, Figure 3), it is known that the amount of newly formed phase is approximately the same as that of the unreacted MoO_3(4,4′-bipyridyl)$_{0.5}$. As revealed by XRD, the reduction in inter-basal-plane distance indicates a configuration change for 4,4′-bipyridine ligands. Because our XPS analysis (Table 1) has confirmed the formation of MoS_2 slabs (whose van der Waals thickness is 0.62 nm) at 250 °C, the interlayer space for 4,4′-bipyridine intercalant can be further attained: 1.02 nm − 0.62 nm = 0.40 nm. This space is obviously too small for a standing 4,4′-bipyridine which has a vertical dimension of ca. 0.88 nm.[49] Furthermore, considering only ═$N^{\delta+}$− species (401.2 eV) are shown in the N 1s spectra, a more stable interlayer arrangement of the detached 4,4′-bipyridine molecules may be attained upon this configuration transformation. In this agreement, a strong attenuation/broadening in IR absorptions (Figure 2c) indicates a greater coupling (solid−state effect) between the MoS_2 sheets and the flat-lying 4,4′-bipyridine intercalants, although their actual structural arrangement (e.g., possible epitaxial or quasi-epitaxial relationship) is still unknown at this stage. According to our XRD results (250 °C, Figure 3), neither the bulk 2H−MoS_2 nor the normal SML−MoS_2 (SML = single-molecular-layer)[91,92] are formed at this temperature, which rules out the bulk intermolecular sheet condensation (agglomeration) among the resulting MoS_2 slabs, although it could occur in the top surface (will be addressed later in Figure 7d). All these observations indicate that the 4,4′-bipyridine molecules serve as spacers to insolate individual molecular-sheets of MoS_2 from one another, but unlike in the pristine MoO_3(4,4′-bipyridyl)$_{0.5}$ they do not have direct coordination to the MoS_2 sheets (Figure 1b). Due to their flat-lying configuration, some ($^3/_5$) of the 4,4′-bipyridine molecules have been evaporated at 250 °C. Chemical formula for this resulting new phase has been determined as MoS_2(4,4′-bipyridyl)$_{0.2}$. All these points will be further addressed below.

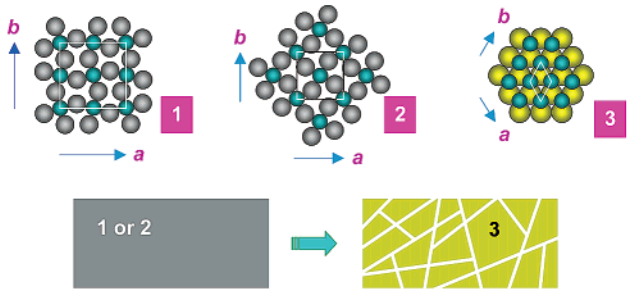

Figure 5. Planar shrinkage and two-dimensional unit-cells in the molecular sheets of: (1) MoO_3(4,4′-bipyridyl)$_{0.5}$, a = 0.75727 nm, b = 0.73675 nm, and β = 90.396°;[49] (2) H_xMoO_3-(4,4′-bipyridyl)$_{0.5}$, a = 0.52644 nm, b = 0.52642 nm, and β = 90.035°;[49] and (3) MoS_2(4,4′-bipyridyl)$_{0.2}$, $a = b$ = 0.316 nm, and γ = 120°.[13] Atomic notation is identical to that in Figure 1.

The formation of MoS_2 involves a lateral contraction of Mo−Mo sublattice and therefore the observed planar shrinkage of MoS_2(4,4′-bipyridyl)$_{0.2}$. According to the crystallographic data,[49,52] the atomic specific surface area of Mo takes the following sequence: 0.1395 nm^2/Mo [MoO_3(4,4′-bipyridyl)$_{0.5}$], 0.1386 nm^2/Mo [H_xMoO_3-(4,4′-bipyridyl)$_{0.5}$], and 0.0865 nm^2/Mo [MoS_2(4,4′-bipyridyl)$_{0.2}$], as detailed in Figure 5. Consistent with this area reduction, crystal cracking has been reported in the morphological evolution of Figure 2 for the reacted crystals. For the crystal samples reacted at higher temperatures, more and finer slits of the cracks have been seen in response to the above spatial changes. Figure 6 shows the profiles of relative atomic ratio of the unreacted MoO_3 to total Mo, based on XPS surface detection in this study. As can be seen, the ratio decreases gradually up to 200 °C, after which there is an increase at 250 °C. To explain this, one has to realize that H_xMoO_3 is an intermediate phase formed in the interfacial region between MoS_2 and MoO_3 according to their Mo oxidation states and reaction sequence. At 200 °C, however, although MoO_3 has been observed, its partially reduced phase H_xMoO_3 is not detectable, which seems to contradict our general expectation that H_x-MoO_3 should also be present if both MoO_3 and $MoO_{2-x}S_x$ ($x \leq 2$) are observable. Therefore, the observed MoO_3 phase could only be attributed to the presence of crystal cracks where X-rays can probe directly into the internal bulk MoO_3(4,4′-bipyridyl)$_{0.5}$ (Figure 1b). This postulation is further supported by the reactions of 250 °C at which more crystal cracks are generated, giving rise to a stronger Mo 3d photoelectron signal of the MoO_3 phase (Figure 6). In view of this signal variation and absence of H_xMoO_3 signal for the samples reacted at 200−250

(91) Afanasiev, P.; Xia, G. F.; Berhault, G.; Jouguet, B.; Lacroix, M. *Chem. Mater.* **1999**, *11*, 3216.
(92) Peng, Y.; Meng, Z.; Zhong, C.; Lu, J.; Yu, W.; Jia, Y.; Qian, Y. *Chem. Lett.* **2001**, 772.

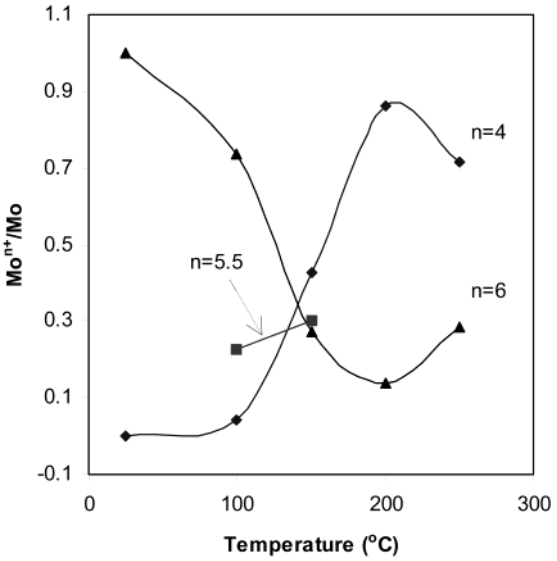

Figure 6. Relative elemental analysis based on peak area ratios of XPS spectra (Figure 4) for as-prepared MoO_3(4,4′-bipyridyl)$_{0.5}$ crystals and their reacted samples in the H_2S/H_2 stream at 100−250 °C for 1 h.

°C, it is suggested that the cracks contributing to the MoO_3 detection were largely developed only during the cooling.

Although our main objective in this work is to investigate the sulfidation process of single-molecular sheets of MoO_3, the conversion of MoO_3(4,4′-bipyridyl)$_{0.5}$ to MoS_2(4,4′-bipyridyl)$_{0.2}$ under the H_2S/H_2 atmosphere virtually represents a new means for fabrication of MoS_2-related organic−inorganic hybrids with gas−solid reactions. In fact, with a reaction time of 6 h at 250 °C, single-phase MoS_2(4,4′-bipyridyl)$_{0.2}$ can be produced, as indicated in the XRD pattern of Figure 7a. A SEM morphological image of MoS_2(4,4′-bipyridyl)$_{0.2}$ and its related EDX spectrum are displayed in Figure 7b,c. As expected, the atomic ratio between Mo and S (0.55 from the EDX result) is close to the theoretical value of 1/2, confirming the stoichiometric ratio of Mo to S in this compound. Furthermore, the content of 4,4′-bipyridine in the MoS_2(4,4′-bipyridyl)$_{0.2}$ has been determined with the CHN method (C/H/N = 11.97 wt %/1.51 wt %/2.68 wt %), which also confirms that the 4,4′-bipyridine molecules do not decompose in this new hybrid compound. Lattice fringes (TEM image, Figure 7d) of this sample powder indeed show a layered structure. There are two types of inter-sheet distances observed. The first one, with a value of 1.00 nm, is in excellent agreement with the d_{001}, derived from the XRD method. The second one, observed merely among the topmost layers, has a value of 0.62 nm which is identical to the basal distance d_{002} of 2H−MoS_2. This finding reveals that the removal of 4,4′-bipyridine intercalants has occurred in the surface region at this temperature, although the massive elimination (deintercalation) of 4,4′-bipyridine in the bulk phase takes place only at 315 °C based on our TGA experiments in nitrogen atmosphere. During the sulfidation or removal of 4,4′-bipyridine, the crystal network does suffer sequential changes because of lattice parameter changes, which results in the smaller and fragmented MoS_2 slabs observed from the above TEM image (also refer to Figure 5). Figure 7e displays a ring-like SAED pattern for the final MoS_2(4,4′-bipyridyl)$_{0.2}$ phase, showing that the overall sample is indeed largely amorphous, although some diffraction spots can be seen. The average crystallite size (after powdering) calculated for MoO_3(4,4′-bipyridyl)$_{0.5}$ is in the range of 50−65 nm along [001] direction, whereas the same dimension for MoS_2(4,4′-bipyridyl)$_{0.2}$ is only 19−22 nm using Scherrer's method and the XRD fwhm data of Figures 2 and 7a. This crystalline dimension reduction can be attributed to *d*-spacing variation between the two compounds, which causes MoS_2(4,4′-bipyridyl)$_{0.2}$ to have difficulty finding neighboring layers during the shrinkage along the [001] direction. On the basis of the above work, as well as the literature findings,[51,52] the formation mechanism is further proposed in Figure 8. Owing to a large interlayer space in MoO_3(4,4′-bipyridyl)$_{0.5}$, an HS^- ion can approach the Mo^{6+} center easily (step 1). In weakening the original Mo−N coordination bond, H−S^- and O−Mo then form a transition-state of four-centered ring-species (step 2) via hydrogen bonding between H and O, which will further weaken the Mo−N bond and replace the 4,4′-bipyridine coordination to the central atom Mo (step 3). Repeating steps 1−3 will eventually lead to the formation of MoS_2(4,4′-bipyridyl)$_{0.2}$ phase (step 4). It is believed to be synergism-beneficial that the intercalated 4,4′-bipyridine molecules, being highly aromatic in nature, will interact noncovalently with the hexagonally packed MoS_2 slabs using the π-electrons of their six-member-rings while interacting via hydrogen bonds (e.g., S···H and C···H) for their intermolecular self-organization. This explanation is also in agreement with the observed negative BE shift of the metal cations (Mo 3d, Table 1) in the host layers, and the positive BE shifts of nonmetal guest species (C 1s and N 1s, Table 1) in the interlayer space at higher reaction temperatures.

Further detailed structural determination on MoS_2 sheets appears to be challenging. For example, 2H−MoS_2 to 1T−MoS_2 (in which Mo is located in an octahedral site formed by six S atoms) transformation has been often observed in exfoliated single molecular sheets of MoS_2. This transformation has been ascribed to the charge transfer from the alkali metal atoms to the MoS_2 host.[33] Compared to alkali metal intercalants, nevertheless, it has been known that the interaction between pyridyl compounds and MoS_2 sheets is much weaker;[88] we will further address these issues in our future investigations.

Conclusion

In summary, single molecular sheets of MoO_3 in MoO_3-containing layered compounds can be viewed as 2D inorganic "macromolecules" supported by (or suspended by) organic "pillars" (or "threads"). In the present example, we have demonstrated that formation of surface H_xMoO_3(4,4′-bipyridyl)$_{0.5}$ from its precursor MoO_3(4,4′-bipyridyl)$_{0.5}$ can be started at a temperature as low as 100 °C under a reducing reaction atmosphere of H_2S/H_2. The surface $MoO_{2-x}S_x$ and elemental S, produced from the sulfurization reactions, are also found in the temperature range of 100−200 °C. When the temperature is raised to 250 °C, all the observed intermediate phases (predominantly in $MoO_{2-x}S_x$) are sulfurized completely to a metal−dichalcogenide−organic hybrid compound MoS_2(4,4′-bipyridyl)$_{0.2}$. On the

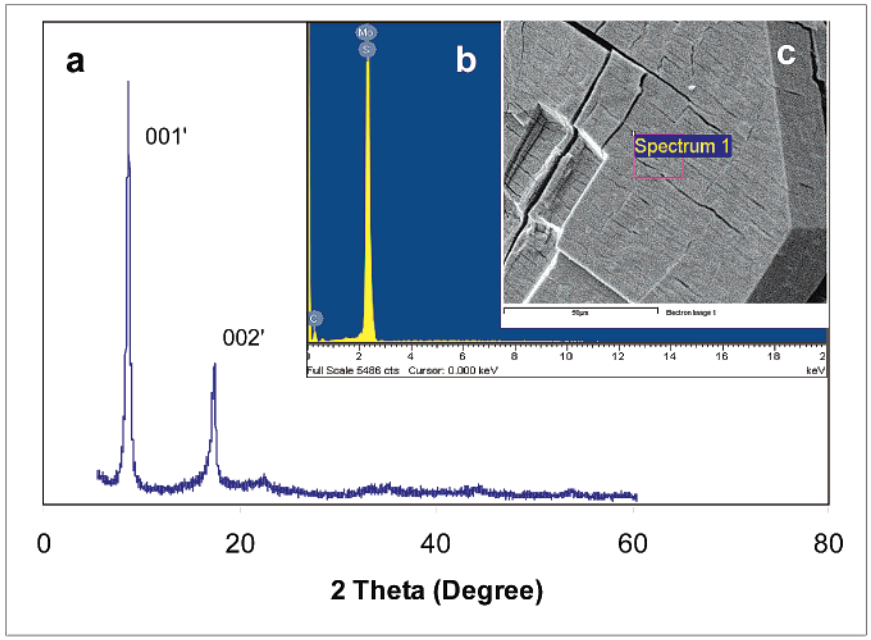

Figure 7. XRD pattern (a), EDX spectrum (b), SEM image (c) related to (b), TEM image (d), and SAED pattern (e) for a single-phase MoS_2(4,4′-bipyridyl)$_{0.2}$ produced from sulfidation of MoO_3(4,4′-bipyridyl)$_{0.5}$ in the H_2S/H_2 stream at 250 °C for 6 h.

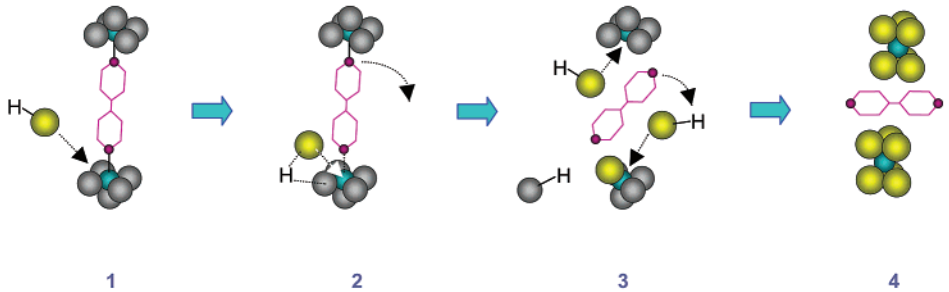

Figure 8. Proposed sulfidation mechanism of MoO_3(4,4′-bipyridyl)$_{0.5}$ and/or H_xMoO_3(4,4′-bipyridyl)$_{0.5}$ to MoS_2(4,4′-bipyridyl)$_{0.2}$. Atomic notation is identical to that in Figure 1.

basis of observed basal spacing reduction (from 1.12 to 1.02 nm; 8.9% reduction), it is understood that 4,4′-bipyridine ligands in the interlayer space underwent a standing-to-lying configuration transformation, and a partial deintercalation at 250 °C. Furthermore, N 1s photoelectrons show a positive binding energy shift,

indicating an electron transfer of 4,4′-bipyridine to adjacent chemical species upon the sulfidation. The final MoS_2(4,4′-bipyridyl)$_{0.2}$ is thermally stable at its formation temperature (250 °C), whereas the massive deintercalation of 4,4′-bipyridine in nitrogen atmosphere is only observed at 315 °C. Inter-slab condensation of MoS_2 (basal spacing $d_{002} = 0.62$ nm) is also observed on the topmost surface of MoS_2(4,4′-bipyridyl)$_{0.2}$, which may be attributed to surface stripping under the purge of the reaction stream. The estimated average crystallite size of MoO_3(4,4′-bipyridyl)$_{0.5}$ (after powdering) along the [001] direction is in the range of 50−65 nm, while the same dimension for MoS_2(4,4′-bipyridyl)$_{0.2}$ powder is only in 19−22 nm. This difference reflects an original *d*-spacing variation between the two compounds during the sulfidation. The easy conversion of single MoO_3 molecular sheets to MoS_2 slabs can be ascribed to a large interlayer space (created by 4,4′-bipyridine ligands) that allows H_2S or its related ions (e.g., HS^-) to access Mo^{VI} cations in the 2D host sheets. As a new alternative, sulfurization of individual molecular sheets of MoO_3 in their organic-intercalated compounds can be further utilized for future fabrication of inorganic−organic nanohybrids constructed from an alternate stacking of lamellar layers of transition metal dichalcogenides and pristine species of organic intercalants.

Acknowledgment. We gratefully acknowledge research funding (R-279-000-064-112 and A/C50384) cosupported by the Ministry of Education and the National Science and Technology Board, Singapore.

CM020781Y